Available online at www.sciencedirect.com
ScienceDirect
Trans. Nonferrous Met. Soc. China 35(2025) 3638−3649
Transactions of Nonferrous Metals Society of China
www.tnmsc.cn

Effect of pre-deformation on microstructure and intergranular corrosion behavior of 2050 Al−Li alloy

Guo-fu XU[1,2], Jing-yun FU[1], Hao-ran LI[1], Meng-jiao LIU[1], Xiao-yan PENG[1,2], Lei TANG[1,2], Yao LI[1]

1. School of Materials Science and Engineering, Central South University, Changsha 410083, China;
2. Key Laboratory of Nonferrous Materials Science and Engineering of Ministry of Education, Changsha 410083, China

Received 5 February 2025; accepted 15 October 2025

Abstract: The intergranular corrosion behavior of 2050 Al−Li alloy subjected to non-isothermal aging (NIA) treatment with varying pre-deformation amounts was investigated. Results indicate that the resistance to intergranular corrosion improves with increasing pre-deformation amouts. However, when the pre-deformation amount reaches 20%, the corrosion resistance deteriorates. Microstructural analyses via transmission electron microscopy (TEM) and electron backscatter diffraction (EBSD) reveal that as pre-deformation amount increases, the fraction of high-angle grain boundaries (HAGBs) decreases, while the proportion of low-angle grain boundaries (LAGBs) increases. This change provides additional nucleation sites for precipitates, leading to a reduction in T_1 phase size and an increase in T_1 phase density. The finer T_1 phases contribute to a lower localized potential difference within the grains, slowering corrosion propagation. Furthermore, during corrosion, preferential dissolution of Li results in Cu enrichment along grain boundaries, which further reduces the intergranular corrosion resistance.

Key words: 2050 Al−Li alloy; intergranular corrosion; microstructure; pre-deformation

1 Introduction

Owing to its light weight, high specific strength and other advantages, Al−Cu−Li alloy has been widely used in aerospace structural parts, such as fuselage and wing chord [1−6]. However, the high reactivity of Li makes Al−Cu−Li alloys highly susceptible to corrosion in specific environments, significantly shortening their service life. Common forms of corrosion include spot corrosion [7], intergranular corrosion [8], exfoliation corrosion [9] and stress corrosion [10]. Among them, intergranular corrosion is a phenomenon of local destruction of alloy materials caused by the action of microbatteries, which involves the corrosion of metal materials along the grain boundary in a specific corrosive medium. This corrosion is extremely destructive to the material. The mechanism of intergranular corrosion mainly includes the theory of depletion, the theory of second phase precipitation [11], the theory of grain boundary adsorption and the theory of stress. The main strengthening phase T_1 (Al_2CuLi) of Al−Li alloy tends to precipitate and coarsen at defects such as grain boundaries and dislocations during aging [12]. The high chemical activity of Li element causes the preferential dissolution of this phase as an anode in the corrosion cell, resulting in intergranular corrosion [13]. Moreover, grain boundary is more likely to absorb impurities or act as the nucleation site of coarse and insoluble second. phase particles due to its high energy. These features can disrupt the integrity of the passive film,

Corresponding author: Yao LI, Tel: +86-18773352271, E-mail: 22024017@csu.edu.cn
https://doi.org/10.1016/S1003-6326(25)66903-2

making such regions preferential sites for localized corrosion [14]

Extensive research has been conducted on the intergranular corrosion of Al−Li alloys. WANG et al [8] studied the effect of grain structure on the intergranular corrosion properties of Al−Cu−Li alloys. It is found that T6-aged 2A97 Al−Cu−Li alloy is prone to grain boundary corrosion and subgrain boundary corrosion, and the local corrosion occurs and extends along the sub-boundary. LIN et al [15] studied the effect of aging treatment on the intergranular corrosion properties of Al−Cu−Li alloys. Their results demonstrated that T8 two-stage aging can effectively reduce the intergranular corrosion sensitivity of Al−Cu−Li alloy. A high density of finely distributed T_1 precipitates within the grains, along with a discontinuous distribution of grain boundary precipitates, reduced the corrosion potential difference between the matrix and the grain boundaries, thereby improving intergranular corrosion resistance. LIU et al [16] studied the effect of pre-strain coupled cryogenic aging on the corrosion behavior of 2A97 Al−Li alloy. It was found that pre-strain inhibits the precipitation of T_1 phase and δ' phase at the grain boundary and prevents the formation/expansion of precipitation-free zone. This process reduces the potential difference between the grain boundaries and the matrix, enhancing the alloy's corrosion resistance. However, most studies have focused on the roles of HAGBs, LAGBs, and precipitate distributions on the corrosion behavior. The fundamental cause of corrosion, namely the electrochemical potential differences resulting from variations in chemical composition across different microstructural regions, has less been thoroughly investigated.

Therefore, the research of corrosion behavior of 2050 Al−Li alloy should not be limited to grain boundary composition and structure. Furthermore, non-isothermal aging (NIA) treatment applied to 2050 Al−Li alloy with varying pre-deformation levels leads to the precipitation of T_1 phases with different sizes. The variations in the chemical composition of these T_1 phases induce micro-scale potential differences within the matrix, ultimately influencing corrosion resistance. This study provides a detailed characterization and discussion of this phenomenon.

2 Experimental

2.1 Materials and heat treatment

The material used in the experiment is 2050 Al−Li alloy sheet with 27 mm in thickness after pre-deformation treatment provided by a domestic company. The experimental plates were first annealed at 525 °C for 4 h and then rolled to 5 mm in multiple passes on a two-high hot mill. After annealing at 525 °C for 1 h, the hot-rolled plate was air-cooled to room temperature and cold-rolled to 2 mm in thickness by multiple passes. The thin plate was cut into 15 mm × 15 mm square samples by wire cutting machine, and the solid solution treatment was carried out at 525 °C for 1 h, and the samples were immediately water-quenched after solid solution treatment. After quenching, the samples were pre-deformed by cold rolling with different deformation amounts, which were 0, 4%, 8%, 12%, 16% and 20%, respectively. Non-isothermal aging (NIA) was performed on the sample after rolling pre-deformation treatment, and the NIA system is shown in Fig. 1. The sample was first heated from 130 to 220 °C at a rate of 30 °C/h, then cooled to 130 °C at the same rate, and sampled at 150 °C. The NIA process has been optimized in previous studies [17].

2.2 Intergranular corrosion test

The intergranular corrosion test was conducted according to GB/T 7998—2005 standard [8,15,18]. Before the intergranular corrosion test, the specimen was polished with sandpaper first and then mechanically polished until there were no visible scratches on the surface. The intergranular corrosion solution was a mixture of 57 g/L NaCl + 10 mol/L H_2O_2 (1.1 g/mL). The experiment was carried out in a constant temperature water bath at (35±2) °C, and the impregnation time was 6 h.

2.3 Microstructure characterization

The intergranular corrosion sample was cut in the middle along the end perpendicular to the rolling direction, and the morphology of intergranular corrosion was observed by DMILM inverted optical microscope (OM). The sample was first mounted with epoxy resin, then polished with sandpaper, and finally mechanically polished until there were no obvious scratches on the surface.

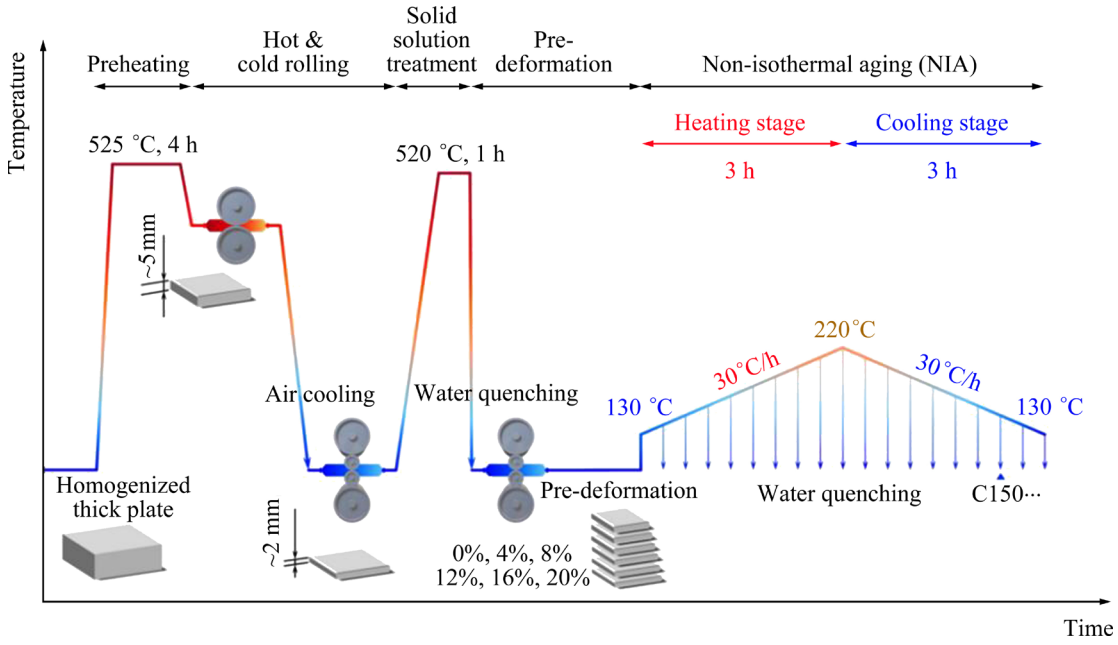

Fig. 1 Schematic diagram of heat treatment process for 2050 Al−Li alloy

The electron backscatter diffraction (EBSD) of FEI Sirion 200 field emission scanning electron microscope (SEM) was used to observe the grain morphology and the corrosion path of the intergranular corrosion samples. The EBSD sample of the non-corroded sample was observed on the transverse direction−normal direction (TD−ND) surface, and the sample was first polished with sandpaper and mechanically polished until there was no obvious scratch on the surface, and then electrolytically polished. The electrolytic polishing liquid was a mixed solution of 10% perchloric acid and 90% ethanol, the experimental temperature was −20 °C, the voltage was 10 V, and the polishing time was 60−90 s. In order to avoid affecting the observation of corrosion path of corrosion samples, the intergranular corrosion EBSD samples with different pre-deformation amounts was firstly mechanically polished, and then thinned by Gatan 691 ion thinning instrument with electron beam energy of 5 keV and thinning angle of 8°. EBSD data were analyzed by TSL OIM software. High-angle grain boundaries (HAGB, 15°−180°) were marked by black lines, and low angle grain boundaries (LAGB, 3°−15°) were marked by white lines.

The precipitation behavior was observed by FEI Tecnai G^2 F20 S-Twin field emission transmission electron microscope (TEM) equipped with a high-angle annular dark field (HAADF) detector. The operating voltage was 200 kV. The TEM specimen was polished to 50−70 μm, then mechanically polished, and finally the *d*3 mm disc was rinsed for electrolytic double spraying. The electrolysis double spray solution was a mixed solution of 30% HNO_3 and 70% CH_3OH, and the temperature was about −25 °C.

3 Results

3.1 Intergranular corrosion

Figure 2 presents OM images illustrating the intergranular corrosion behavior of the 2050 Al−Li alloy with various pre-deformation amounts after by NIA. The maximum intergranular corrosion depth reached 132 μm without pre-strain. The increase of pre-deformation (at low strain conditions) could effectively decrease the intergranular corrosion depth. When the pre-deformation increased to 16%, the intergranular corrosion depth reached a minimum of 20 μm. However, when the amount of pre-deformation further increased to 20%, the intergranular corrosion depth increased to 81 μm.

3.2 EBSD results

Figure 3 shows the EBSD diagrams of TD−ND surface of 2050 Al−Li alloy with different

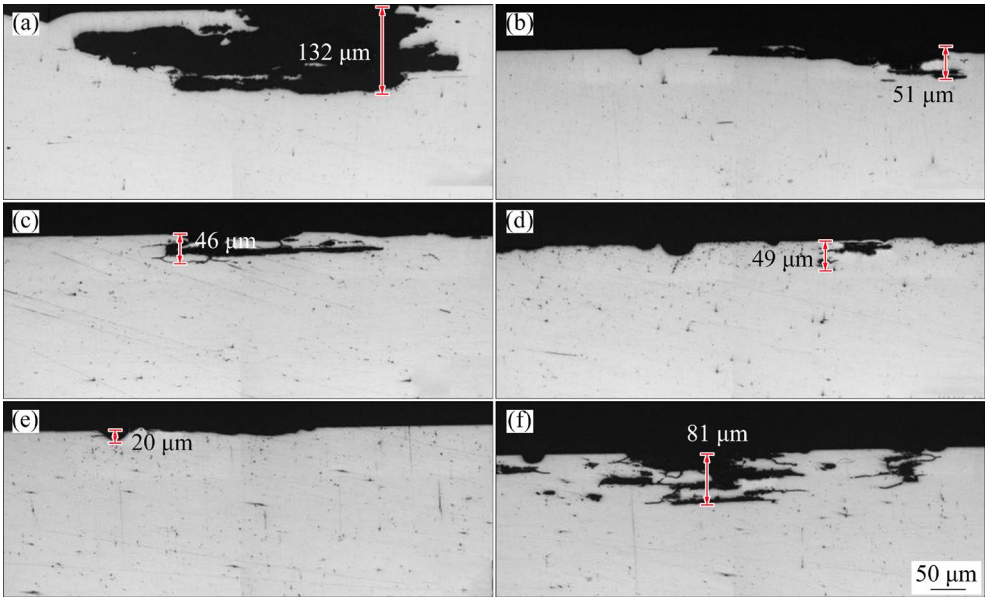

Fig. 2 OM images of intergranular corrosion of 2050 Al−Li alloy with different pre-deformation amounts after NIA treatment: (a) 0; (b) 4%; (c) 8%; (d) 12%; (e) 16%; (f) 20%

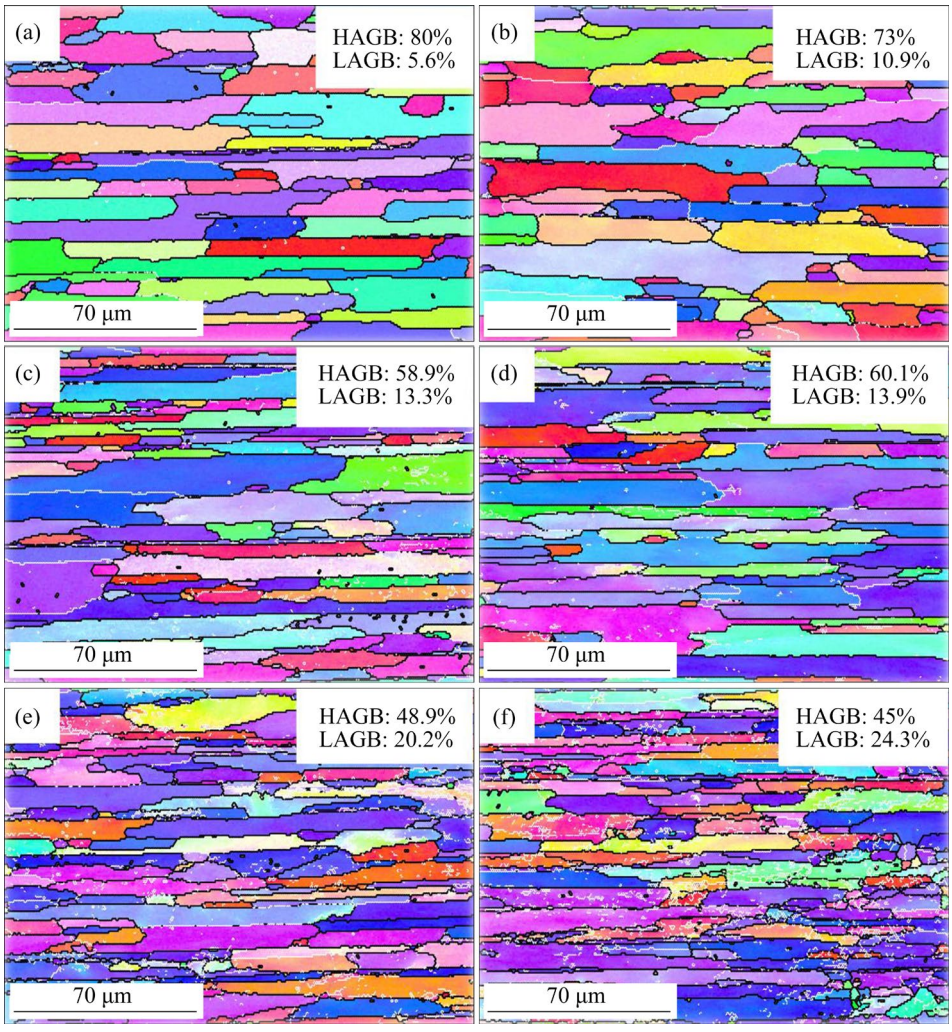

Fig. 3 EBSD diagrams of TD−ND surface of 2050 Al−Li alloy with different pre-deformation amounts: (a) 0; (b) 4%; (c) 8%; (d) 12%; (e) 16%; (f) 20%

pre-deformation amounts. The grain was elongated along the TD direction, and the grain size gradually decreased along the ND direction with the increase of pre-deformation amount. In addition, with the increase of pre-deformation amounts, the proportion of HAGB gradually decreased, while the proportion of LAGB gradually increased. When the amount of pre-deformation gradually increased to 16%, the proportions of HAGB and LAGB were 48.9% and 20.2%, respectively.

Figure 4 shows the grain orientation spread (GOS) diagrams of TD−ND surface of 2050 Al−Li

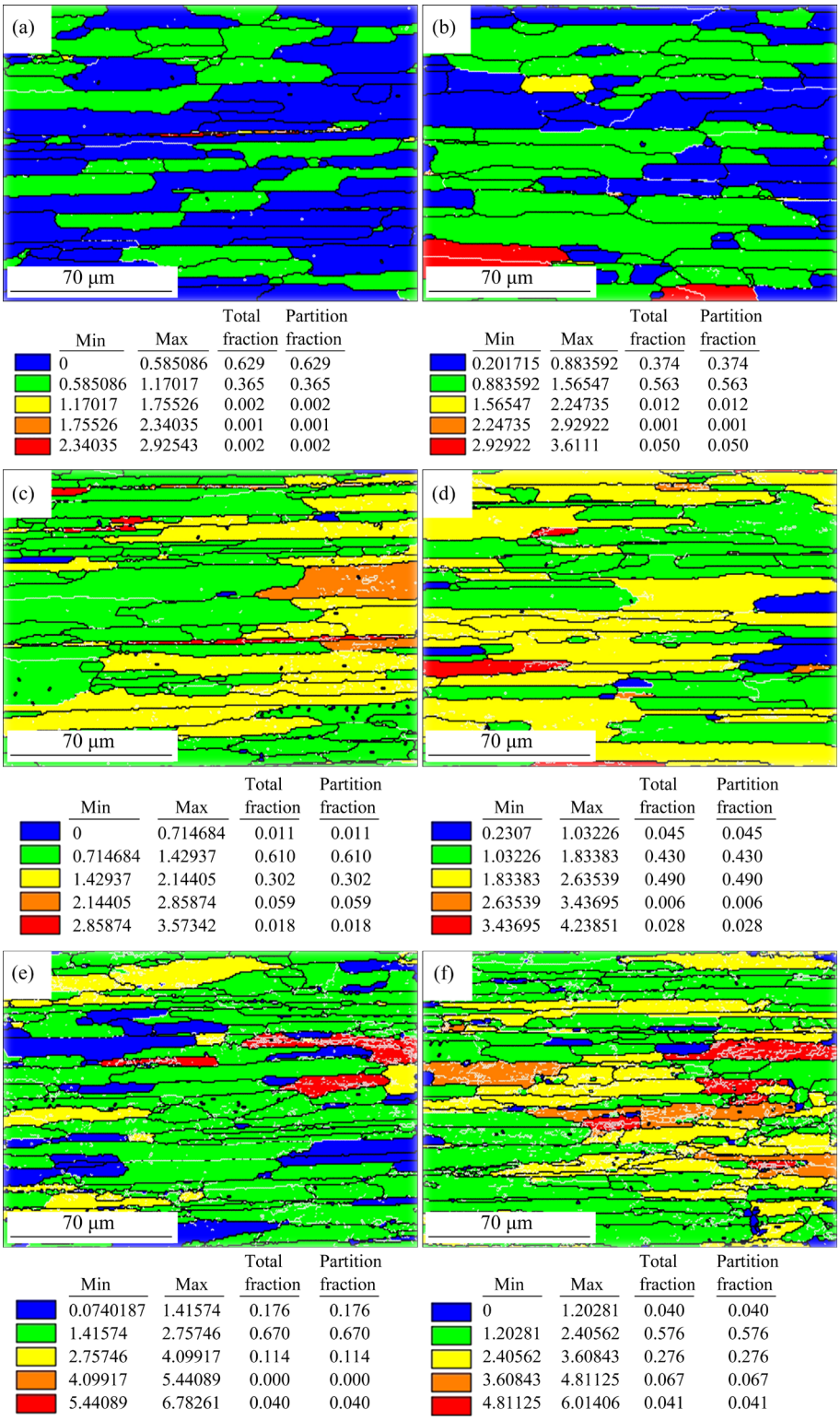

Fig. 4 GOS diagrams of TD−ND surface of 2050 Al−Li alloy with different pre-deformation amounts: (a) 0; (b) 4%; (c) 8%; (d) 12%; (e) 16%; (f) 20%

alloy with different pre-deformation amounts. GOS quantifies the deviation in orientation between each pixel within a grain and the average orientation of that grain. Each grain is colored based on the mean misorientation value across all constituent pixels, thereby reflecting the local strain level through the degree of lattice rotation. As shown in Fig. 4, the transition in grain color from blue to red corresponds to an increase in grain strain. Without pre-deformation, the GOS value was mainly in the range of 0−3, indicating a small intracrystalline distortion. With the application of the pre-deformation, the GOS value increased significantly. The GOS value reached the maximum of 6.7 when the pre-deformation increased to 16%. As the pre-deformation amount further increased to 20%, although the maximum GOS value was only 6.01, the distortion distribution within the grain was more uniform, resulting in the highest average GOS value under all conditions.

The EBSD diagrams of NIA 2050 Al−Li with different pre-deformation amounts after intergranular corrosion test are shown in Fig. 5. In the absence of pre-deformation (0%), the intergranular corrosion was mainly along the grain boundary, though serious corrosion also occurred in some grains. When the amounts of pre-deformation were 8% and 20%, intergranular corrosion occurred mainly along grain boundaries, as shown in Fig. 5(b). Notably, when the amount of pre-deformation was 12%, intergranular corrosion mainly occurred within the grain, as shown in Fig. 5(c).

3.3 TEM analysis results

Figure 6 shows dark-field TEM images of 2050 Al−Li alloy with different pre-deformation amounts after NIA treatment in ⟨112⟩ direction. When the pre-deformation amount was 0, the precipitates size was large and the number density was small. Selected-area electron diffraction (SAED) patterns confirmed that the T_1 phase was the predominant precipitate. When pre-deformation was performed before aging, the size of precipitates

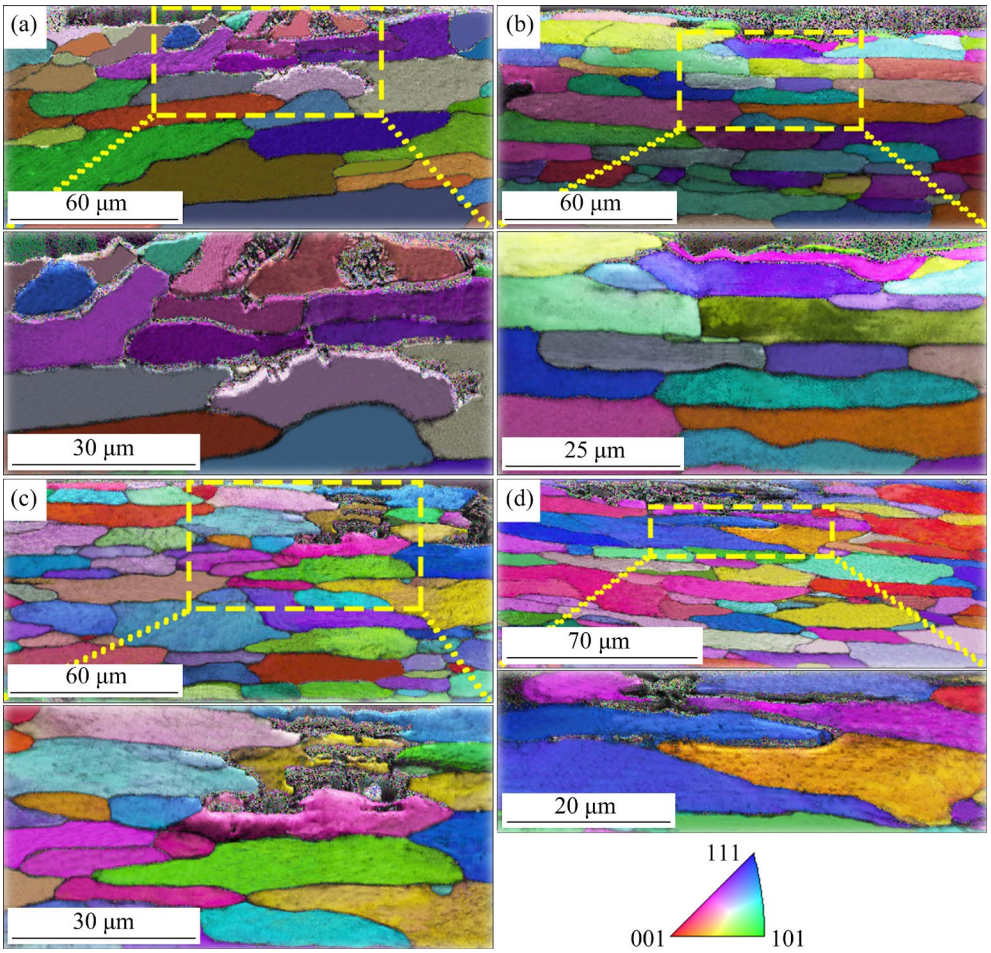

Fig. 5 EBSD diagrams of intergranular corrosion of 2050 Al−Li alloy with different pre-deformation amounts after NIA treatment: (a) 0; (b) 8%; (c) 12%; (d) 20%

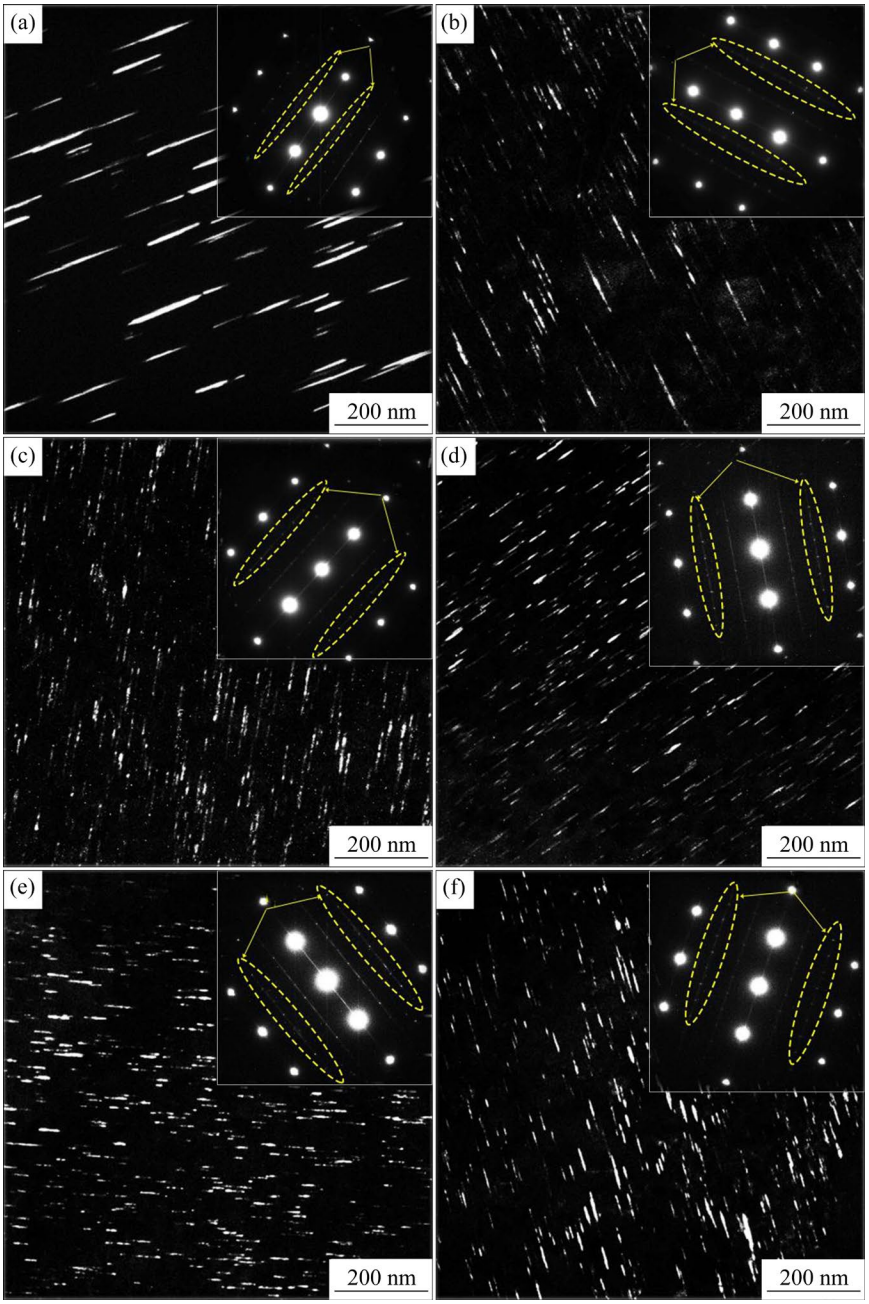

Fig. 6 TEM images of 2050 Al−Li alloy with different pre-deformation amounts after NIA treatment in ⟨112⟩ direction: (a) 0; (b) 4%; (c) 8%; (d) 12%; (e) 16%; (f) 20%

decreased and the number density increased obviously, as shown in Fig. 6(b). The size of precipitates continued to be refined and the number density continued to increase with further increase of pre-deformation amounts. At 16% pre-deformation, the precipitate size reached a minimum while the number density attained its maximum. However, with the further increase of the pre-deformation amount to 20%, the size of the precipitates increased and the number density decreased.

Figure 7 shows the typical bright-field TEM images of grain boundaries of 2050 Al−Li alloy with different pre-deformation amounts after NIA treatment. Without pre-deformation, the grain boundary precipitates (GBPs) were small and continuously distributed, as shown in Fig. 7(a). With the introduction of pre-deformation treatment, GBPs were obviously coarsened and distributed discontinuously, as shown in Figs. 7(c, d). At 16% pre-deformation, the GBPs displayed a semi-continuous distribution, with both continuous and

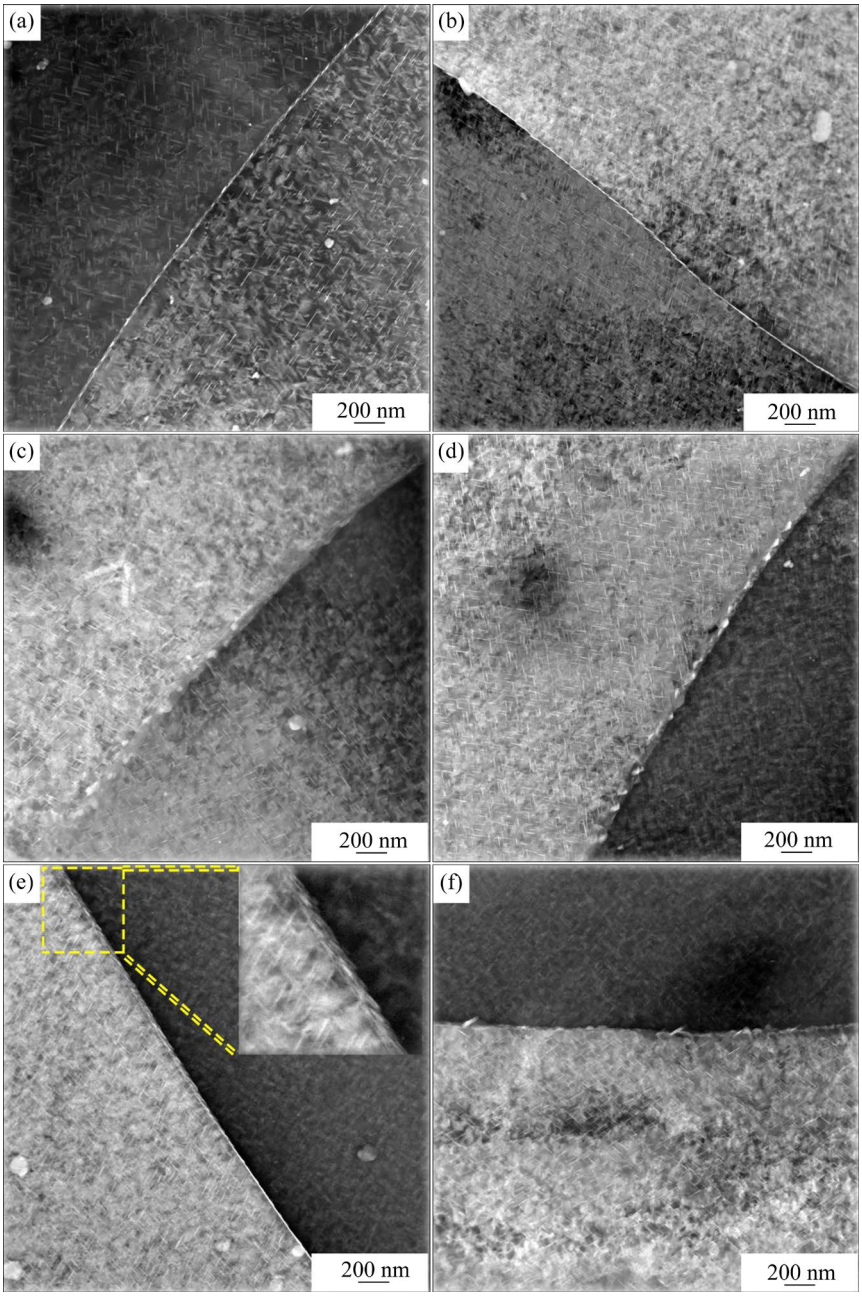

Fig. 7 TEM images of grain boundaries of 2050 Al−Li alloy with different pre-deformation amounts after NIA treatment: (a) 0; (b) 4%; (c) 8%; (d) 12%; (e) 16%; (f) 20%

discontinuous segments. When the pre-deformation amount was further increased to 20%, the GBPs again had a discontinuous distribution, as illustrated in Fig. 7(f).

Figure 8 illustrates the coarsening process of the T_1 phase and presents energy-dispersive spectroscopy (EDS) analysis of the phase before and after coarsening. It could be seen that coarsening of the T_1 phase primarily involved thickening, and the thickness of T_1 phase increased from 1.78 to 2 nm. Due to the low atomic number of Li element, it could not be detected by EDS. The EDS analysis confirmed that the T_1 phase consisted mainly of Al and Cu. The thickening of the T_1 phase corresponded to the addition of more than one atomic layer of Cu.

4 Discussion

4.1 Effect of pre-deformation on precipitation behavior of 2050 Al−Li alloy

Pre-deformation refers to the process of plastically deforming an alloy following solution treatment and quenching but prior to aging. In Al−Li

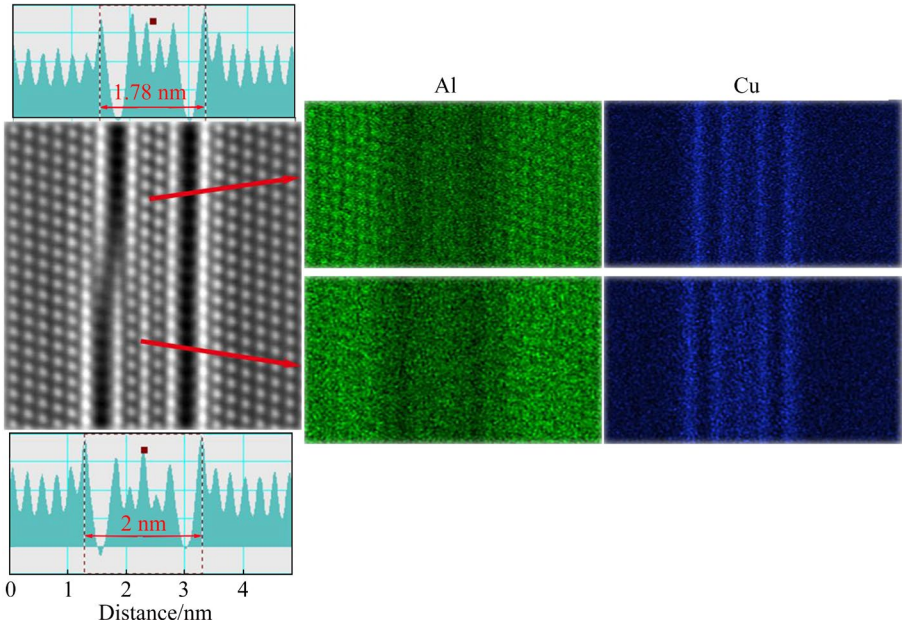

Fig. 8 T_1 phase coarsening process and energy spectrum analysis of different size T_1 phases

alloys containing multiple precipitate phases, the formation of various precipitates is often competitive, and pre-deformation significantly influences this precipitation behavior. For example, pre-deformation of Al−Cu−Li alloys prior to aging can promote T_1 phase precipitation at the expense of other precipitates (θ' phases and δ' phases) [19−22]. This indicates that the promotion of T_1 phase precipitation by pre-deformation is more dominant than that of other phases. As shown in Fig. 6, the main precipitated phase of 2050 Al−Li alloy after pre-deformation treatment and NIA treatment is T_1 phase.

Moreover, in addition to influencing intragranular precipitation, pre-deformation also mitigates competitive nucleation and growth of precipitates at grain boundaries. This suppression helps inhibit the formation of precipitate-free zones (PFZs) adjacent to grain boundaries, reduces the stress concentration, and thereby improves the corrosion resistance of the alloy [23]. The pre-deformation introduces work hardening, and the resulting mobile dislocations promote fine and homogeneous nucleation of strengthening phases, particularly since the T_1 phase preferentially nucleates at defects such as dislocations, grain boundaries, and vacancies [24]. As shown in Fig. 3, without pre-deformation, the alloy exhibits relatively coarse grains along the TD–ND plane. The proportion of HAGBs is relatively high, and there are fewer dislocation and subgrain boundaries in this case. Under these conditions, the number of nucleation sites is low, leading to coarse T_1 precipitates and a low number density, as shown in Fig. 6(a). With the application of pre-deformation, the grain size decreases noticeably, and the fraction of low-angle grain boundaries (LAGBs) increases progressively (Figs. 3(b−f)). In addition, with the increase of pre-deformation amount, the stress level in the grain increases gradually, and the orientation difference between adjacent pixels increases. As shown in Fig. 4, GOS value gradually increases with the increase of pre-deformation amount. At this time, the nucleation site in the crystal increases, the amount of precipitates increases with the same aging time, and the size of precipitates decreases significantly under the premise of a certain volume fraction, as shown in Figs. 6(b−f).

When the pre-deformation amount reaches 16%, the average size of T_1 phase reaches the minimum and the number density reaches the maximum. However, when the pre-deformation amount further increases to 20%, the average size of T_1 phase increases and the number density decreases, as shown in Fig. 6(f). This reversal is attributed to the formation of a cellular dislocation structure due to severe deformation: dislocation walls exhibit high dislocation density, while the cell interiors remain relatively dislocation-free. T_1 phase preferentially nucleates along these cell walls,

leading to a reduced nucleation rate. Additionally, the high stored energy near the dislocation walls provides a driving force for precipitate growth. The formation of dislocation cells leads to a more uneven distribution of dislocations. The T_1 phase can preferentially nucleate at the walls of dislocation cells with greater storage capacity, while at other locations without dislocations, the nucleation and precipitation of the T_1 phase are less. Furthermore, the content of alloying elements within the matrix is fixed. As the aging process progresses, the T_1 phase that initially precipitates can preferentially grow and become coarser. Therefore, the precipitated T_1 phase is relatively coarse, and the distribution uniformity decreases.

4.2 Effect of pre-deformation on corrosion behavior of 2050 Al−Li alloy

Intergranular corrosion means that the corrosion occurs from the surface near the grain boundary and extends into the grain interior. There are no obvious signs of corrosion on the surface, but the binding force among the grains is severely weakened, resulting in a decrease in the strength of the alloy. The generally accepted mechanism of intergranular corrosion of Al alloy mainly includes the following three theories: (1) galvanic corrosion caused by the potential difference between the matrix and grain boundary precipitates [25], and (2) the difference in breakdown potential between the matrix and grain boundary precipitates [26,27]. The dissolution of grain boundary precipitates forms an aggressive occluded medium that sustains intergranular corrosion [28,29]. In summary, the intergranular corrosion of Al−Li alloy is caused by the potential difference between different parts of the alloy, especially between the grain boundary and the grain, and between the precipitated phase and the matrix. The research [30,31] also shows that there is an obvious potential difference between grain boundary and matrix, and the potential difference is caused by the uneven distribution of alloying elements. The results show that in Al−Li alloy, due to the higher positive electrode potential of Cu relative to Al, the Cu-containing precipitated phase (T_1 phase), Cu-rich nanoparticles, Cu-rich layer and Cu segregation at the grain boundary are all considered to be effective cathodes to promote the dissolution of the peripheral anode of Al, resulting in intercrystalline corrosion [32].

In addition, the main precipitated phase in 2050 Al−Li alloy is T_1 phase. While T_1 phase contains Li element, Li element can dissolve preferentially during the corrosion process, making the remaining part of T_1 phase rich in Cu during the corrosion process, causing the potential to move in a positive direction. This Cu-enriched T_1 phase then acts as a cathode and promotes anodic dissolution of the surrounding matrix [33]. Therefore, when the amount of pre-deformation is 0, the number of nucleation sites is limited, resulting in a low density of coarse intragranular precipitates. These large precipitates introduce significant localized potential differences within the matrix. Furthermore, the continuous network of grain boundary precipitates (Fig. 7(a)) provides a facile path for corrosion penetration, explaining the poor corrosion resistance observed in Fig. 2(a). The larger size of grain boundary precipitates compared to those within grains also leads to a greater potential difference near grain boundaries, favoring corrosion propagation along these boundaries, as shown in Fig. 5(a). With the increase of pre-deformation amount, the energy storage of the alloy increases, the nucleation position increases, the size of the precipitates decreases, and the number density increases. During the corrosion process, Li element in T_1 phase corrodes preferentially, the Cu content in the remaining part of T_1 phase is relatively small (Fig. 8), and the potential difference with the matrix is small, which slows down the corrosion process.

In addition, due to the obstruction of dislocation in the pre-deformation process of the grain boundary, the energy storage at the grain boundary increases, and the precipitates can preferentially precipitate during the aging process. Although grain boundary precipitates may coarsen, their isolated distribution disrupts continuous corrosion paths. As a result, corrosion resistance improves with moderate pre-deformation. When the pre-deformation amount increases to 16%, the intergranular corrosion resistance of the alloy reaches the best, and the corrosion depth is only 20 μm. However, when the pre-deformation amount further increases, the dislocation clusters occur and cancel each other, resulting in fewer nucleation locations, an increase in the size and number density of precipitated phase, and therefore a decrease in the resistance to intergranular corrosion, as shown in Fig. 2.

5 Conclusions

(1) The intergranular corrosion resistance of 2050 Al−Li alloy after NIA treatment is improved with the increase of pre-deformation amount. The optimal corrosion resistance is achieved at 16% pre-deformation amount, with a corrosion depth of only 20 μm.

(2) The introduction of pre-deformation before aging can provide a favorable position for the nucleation and precipitation of T_1 phase. With the increase of nucleation position, T_1 phase size decreases and its number density increases. However, when the pre-deformation amount reaches 20%, the dislocation clusters occur and cancel each other, which is not conducive to T_1 phase precipitation.

(3) Coarsening of the T_1 phase occurs primarily through thickening, involving the addition of Cu atomic layers. During corrosion, the preferential dissolution of Li leads to the formation of Cu-enriched remnants of the T_1 phase, which acts as efficient cathodes and promotes the anodic dissolution of the adjacent Al matrix, thereby accelerating intergranular corrosion.

CRediT authorship contribution statement

Guo-fu XU: Supervision, Project administration; **Jing-yun FU:** Data curation; **Hao-ran LI:** Data curation; **Meng-jiao LIU:** Data curation; **Xiao-yan PENG:** Supervision; **Lei TANG:** Supervision; **Yao LI:** Data curation, Investigation, Writing − Original draft.

Declaration of competing interest

The authors declare that they have no known competing financial interests or personal relationships that could have appeared to influence the work reported in this paper.

Acknowledgments

This investigation was financially supported by the Postdoctoral Fellowship Program of CPSF, China (No. GZC20242033), and the National Science and Technology Research Program of China (No. JPPT2023PXY01).

References

[1] RIOJA R J, LIU J. The evolution of Al−Li base products for aerospace and space applications [J]. Metallurgical & Materials Transactions A, 2012, 43: 2012−3325.

[2] GUPTA R K, NAYAN N, NAGASIREESHA G, SHARMA S C. Development and characterization of Al−Li alloys [J]. Materials Science and Engineering A, 2006, 420: 228−234.

[3] WILLIMAS J C, STARKE E A. Progress in structural materials for aerospace systems [J]. Acta Materialia, 2003, 51: 5775−5799.

[4] FU Rong, XU Dong, ZHENG Bing, HUANG Yuan-chun, LIU Yu, ZHENG Lei, PANG Hong-xuan, MA Bao-jun. Effect of pre-stretching deformation on the relationship between microstructure, mechanical properties and anisotropy of extruded 2195 Al−Li alloy [J]. Journal of Alloys and Compounds, 2025, 1039: 183260.

[5] MERIC C. Physical and mechanical properties of cast under vacuum aluminum alloy 2024 containing lithium additions [J]. Materials Research Bulletin, 2000, 35: 1479−1494.

[6] XU Guo-fu, LIU Meng-jiao, LIU Shi-chao, TANG Lei, LI Yao, LI Han-ran, LI Jin-feng. Achieving high mechanical and corrosion properties of AA2050 Al−Li alloy: The creep aging under plastic loading [J]. Engineering Fracture Mechanics, 2024, 310: 110475.

[7] MOORE K L, SYKES J M, HOGG S C, GRANT P S. Pitting corrosion of spray formed Al−Li−Mg alloys [J]. Corrosion Science, 2008, 50: 3221−3226.

[8] WANG Xaio-ya, LI Guo-ai, HE Qi-yao, JIANG Jian-tang, LI Dong-feng, SHAO Wen-zhu, ZHEN Liang. Intergranular corrosion of an Al−Cu−Li alloy: The influence from grain structure [J]. Corrosion Science, 2023, 211: 110845.

[9] WANG Xue-hui, WANG Ji-hui, YUE Xin, GAO Yun. Effect of aging treatment on the exfoliation corrosion and stress corrosion cracking behaviors of 2195 Al−Li alloy [J]. Materials & Design, 2015, 67: 596−605.

[10] LIU De-jun, TIAN Gan, YANG Zheng-wei, JIN Guo-feng, ZHANG Wei, WANG Yin, WEI Hua-li. Stress corrosion behavior of 2195-T8 Al−Li alloy with an artificial pit exposed to a 30 vol.% HNO_3 solution [J]. Chinese Journal of Aeronautics, 2023, 36: 304−315.

[11] LI Jin-feng, ZHEN Zi-qiao, REN Wen-da, CHEN Wen-jing, ZHAO Xu-shan, LI Shi-chen. Simulation on function mechanism of $T_1(Al_2CuLi)$ precipitate in localized corrosion of Al−Cu−Li alloys [J]. Transactions of Nonferrous Metals Society of China, 2006, 16: 1268−1273.

[12] XU Guo-fu, LIU Meng-jiao, LIU Shi-chao, TANG Lei, LI Yao, LI Hao-ran, LI Jin-feng. Effect of pre-rolling and aging temperature on the microstructure and mechanical properties of creep-aged 2050 Al−Li alloy [J]. Journal of Materials Research and Technology, 2024, 30: 9037−9047.

[13] LI J F, ZHENG Z Q, LI S C, CHEN W J, REN W D, ZHAO X S. Simulation study on function mechanism of some precipitates in localized corrosion of Al alloys [J]. Corrosion Science, 2007 49: 2436−2449.

[14] LI J F, LI C X, PENG Z W, CHEN W J, ZHENG Z Q. Corrosion mechanism associated with T_1 and T_2 precipitates of Al−Cu−Li alloys in NaCl solution [J]. Journal of Alloys and Compounds, 2008, 460: 688−693.

[15] LIN Yi, LU Chan-ge, WEI Chang-yang, ZHENG Zi-qiao. Effect of aging treatment on microstructures, tensile properties and intergranular corrosion behavior of Al−Cu−Li alloy [J]. Materials Characterization, 2018, 141: 163−168.

[16] LIU Yan, ZHAO Chen-xu, CHEN Jun-feng, LLU Rong-ying, JIANG Jian-tang, CUI Xi-ping, LIANG Si-yan, CHI Hai-tao,

ZOU Lin-chi. Effects of pre-strain deep cryogenic aging on the mechanical and corrosion properties of 2A97 aluminum−lithium alloy [J]. Journal of Materials Research and Technology, 2024, 30: 2728−2737.

[17] LI Yao, XU Guo-fu, PENG Xiao-yan, GUO Guang-yi, LIU Shi-chao, LIANG Xiao-peng. Research on microstructure and mechanical properties of 2050 Al−Li alloy during non-isothermal aging [J]. Journal of Alloys and Compounds, 2022, 906: 163977.

[18] HUANG Jia-lei, LI Jin-feng, LIU Dan-yang, ZHANG Rui-feng, CHEN Yong-lai, ZHANG Xu-hu, MA Peng-cheng, GUPTA R K, BIRBILIS N. Correlation of intergranular corrosion behaviour with microstructure in Al−Cu−Li alloy [J]. Corrosion Science, 2018, 139: 215−226.

[19] LI H Y, KANG W, LU X C. Effect of age-forming on microstructure, mechanical and corrosion properties of a novel Al−Li alloy [J]. Journal of Alloys and Compounds, 2015, 640: 210−218.

[20] GABLE B M, ZHU A W, CSONTOS A A, STARKEJR E A. The role of plastic deformation on the competitive microstructural evolution and mechanical properties of a novel Al−Li−Cu−X alloy [J]. Journal of Light Metals, 2001, 1: 1−14.

[21] RINGER S P, MUDDLE B C, POLMEAR I J. Effects of cold work on precipitation in Al−Cu−Mg−(Ag) and Al−Cu−Li−(Mg−Ag) alloys [J]. Metallurgical & Materials Transactions A, 1995, 26: 1659−1671.

[22] KIM J D, PARK J K. Effect of stretching on the precipitation kinetics of an Al−2.0Li−2.8Cu−0.5Mg(−0.13Zr) alloy [J]. Metallurgical & Materials Transactions A, 1993, 24: 2613−2621.

[23] TSIVOULAS D, PRANGNELL P B. Comparison of the effect of individual and combined zr and mn additions on the fracture behavior of Al−Cu−Li alloy AA2198 rolled sheet [J]. Metallurgical & Materials Transactions A, 2014, 45: 1338−1351.

[24] GAO Chong, LUAN Yang, YU Jun-chuan, MA Yue. Effect of thermo-mechanical treatment process on microstructure and mechanical properties of 2A97 Al−Li alloy [J]. Transactions of Nonferrous Metals Society of China, 2014, 24: 2196−2202.

[25] MAITRA S, ENGLISH G C. Mechanism of localized corrosion of 7075 alloy plate [J]. Metallurgical Transactions A, 1981, 12: 535−541.

[26] BUCHHEIT R G, MORAN J P, STONER G E. Electrochemical behavior of the T_1 (Al_2CuLi) intermetallic compound and its role in localized corrosion of Al−2%Li−3%Cu alloys [J]. Corrosion Science, 2012, 50: 120−130.

[27] BUCHHEIT R G, WALL F D, STONER G E, MORAN J P. Anodic dissolution-based mechanism for the rapid cracking, preexposure phenomenon demonstrated by aluminum−lithium−copper alloys [J]. Corrosion Science, 1995, 51: 417−428.

[28] ANDERSEN S J, MARIOARA C D, FROSETH A. Crystal structure of the orthorhombic U2-$Al_4Mg_4Si_4$ precipitate in the Al−Mg−Si alloy system and its relation to the β' and β'' phases [J]. Materials Science and Engineering A, 2005, 390: 127−138.

[29] BUCHHEIT R G, MORAN J P, STONER G E. Localized corrosion behavior of alloy 2090-the role of microstructural heterogeneity [J]. Corrosion Science, 2012, 46: 610−617.

[30] TRUEMAN R A, LYNCH P S, BIRBILIS N, MUDDLE C B, KNIGHT P S. Correlations between intergranular stress corrosion cracking, grain-boundary microchemistry, and grain-boundary electrochemistry for Al−Zn−Mg−Cu alloys [J]. Corrosion Science, 2010, 52: 4073−4080.

[31] DENG Ying, YIN Zhi-min, ZHAO Kai, DUAN Jia-qi, HU Jian, HE Zhen-bo. Effects of Sc and Zr microalloying additions and aging time at 120 °C on the corrosion behaviour of an Al−Zn−Mg alloy [J]. Corrosion Science, 2012, 65: 288−298.

[32] ZHAG Xin-xin, JIAO Yan-bin, YU Yang, LIU Bing, HASHIMOTO T, LIU Hong-fang, DONG Ze-hua. Intergranular corrosion in AA2024-T3 aluminium alloy: The influence of stored energy and prediction [J]. Corrosion Science, 2019, 155: 1−12.

[33] ZHANG X, ZHOU X, HASHIMOTO T, LINDSAY J, CIUCA O, LUO C, SUN Z, ZHANG X, TANG Z. The influence of grain structure on the corrosion behaviour of 2A97-T3 Al−Cu−Li alloy [J]. Corrosion Science, 2016, 116: 14−21.

预变形对 2050 Al−Li 合金显微组织和晶间腐蚀行为的影响

徐国富[1,2]，符竞云[1]，李昊然[1]，刘梦姣[1]，彭小燕[1,2]，唐 磊[1,2]，李 耀[1]

1. 中南大学 材料科学与工程学院，长沙 410083；
2. 有色金属材料科学与工程教育部重点实验室，长沙 410083

摘 要：研究了不同预变形量 2050 Al−Li 合金经非等温时效处理后的晶间腐蚀行为。结果表明，随着预变形量的增加，合金的腐蚀性能得到提高。然而，当预变形量增加到 20%时，晶间腐蚀抗力降低。透射电子显微镜和背散射电子衍射等显微组织测试表明，随着预变形量的增加，大角度晶界比例降低，小角度晶界比例增加。析出相的形核位置增加，导致 T_1 相尺寸减小、密度增加。细小的 T_1 相导致晶内局部电势差下降，从而减慢腐蚀进程。此外，在腐蚀过程中 Li 元素的优先腐蚀导致 Cu 元素在晶界处富集，从而降低合金的晶间腐蚀性能。

关键词：2050 铝锂合金；晶间腐蚀；显微组织；预变形

(Edited by Bing YANG)